Monthly Notices
of the
ROYAL ASTRONOMICAL SOCIETY

Mon. Not. R. Astron. Soc. **406,** 187–196 (2010) doi:10.1111/j.1365-2966.2010.16698.x

Parsec-scale SiO emission in an infrared dark cloud

I. Jiménez-Serra,[1,2★] P. Caselli,[1] J. C. Tan,[3] A. K. Hernandez,[3] F. Fontani,[4] M. J. Butler[3] and S. van Loo[1]†

[1]*School of Physics and Astronomy, E.C. Stoner Building, University of Leeds, Leeds LS2 9JT*
[2]*Harvard-Smithsonian Center for Astrophysics, 60 Garden St., Cambridge, MA 02138, USA*
[3]*Department of Astronomy, University of Florida, Gainesville, FL 32611, USA*
[4]*Institut de Radioastronomie Millimétrique, 300 rue de la Piscine, 38406 St. Martin d'Heres, France*

Accepted 2010 March 12. Received 2010 March 12; in original form 2009 November 19

ABSTRACT

We present high-sensitivity 2×4 arcmin^2 maps of the $J = 2 \rightarrow 1$ rotational lines of SiO, CO, ^{13}CO and C^{18}O, observed towards the filamentary infrared dark cloud (IRDC) G035.39−00.33. Single-pointing spectra of the SiO $J = 2 \rightarrow 1$ and $J = 3 \rightarrow 2$ lines towards several regions in the filament are also reported. The SiO images reveal that SiO is widespread along the IRDC (size $\geq$2 pc), showing two different components: one bright and compact arising from three condensations (N, E and S) and the other weak and extended along the filament. While the first component shows broad lines (linewidths of ∼4–7 km s^{-1}) in both SiO $J = 2 \rightarrow 1$ and SiO $J = 3 \rightarrow 2$, the second one is only detected in SiO $J = 2 \rightarrow 1$ and has narrow lines (∼0.8 km s^{-1}). The maps of CO and its isotopologues show that low-density filaments are intersecting the IRDC and appear to merge towards the densest portion of the cloud. This resembles the molecular structures predicted by flow-driven, shock-induced and magnetically-regulated cloud formation models. As in outflows associated with low-mass star formation, the excitation temperatures and fractional abundances of SiO towards N, E and S increase with velocity from ∼6 to 40 K and from $\sim 10^{-10}$ to $\geq 10^{-8}$, respectively, over a velocity range of ∼7 km s^{-1}. Since 8 μm and 24 μm sources and/or extended 4.5 μm emission are detected in N, E and S, broad SiO is likely produced in outflows associated with high-mass protostars. The excitation temperatures and fractional abundances of the narrow SiO lines, however, are very low (∼9 K and $\sim 10^{-11}$, respectively), and consistent with the processing of interstellar grains by the passage of a shock with $v_s \sim 12$ km s^{-1}. This emission could be generated (i) by a large-scale shock, perhaps remnant of the IRDC formation process, (ii) by decelerated or recently processed gas in large-scale outflows driven by 8- and 24-μm sources or (iii) by an undetected and widespread population of lower mass protostars. High-angular-resolution observations are needed to disentangle between these three scenarios.

Key words: stars: formation – ISM: individual objects: G035.39−00.33 – ISM: molecules.

1 INTRODUCTION

Infrared dark clouds (IRDCs) are high-extinction regions viewed against the diffuse mid-infrared (mid-IR) Galactic background (Pérault et al. 1996; Egan et al. 1998). These clouds are cold ($T <$ 25 K; Pillai et al. 2007) and exhibit a range of densities from n(H) $\geq 10^3$ cm^{-3} to $\geq 10^4$–10^5 cm^{-3} in their clumps and cores (Teyssier, Hennebelle & Pérault 2002; Butler & Tan 2009). Since these structures have masses and mass surface densities similar to regions that are known to be forming massive protostars and star clusters, they may represent the initial conditions for massive star and star cluster formation (Rathborne, Jackson & Simon 2006; Ragan, Bergin & Gutermuth 2009; Zhang et al. 2009).

It is well-known that silicon monoxide (SiO) is an excellent tracer of molecular gas processed by shocks. While SiO is heavily depleted on to dust grains in the quiescent gas of dark clouds such as L183 (upper limits of the SiO fractional abundance of $\leq 10^{-12}$; Ziurys, Friberg & Irvine 1989; Requena-Torres et al. 2007), this molecule is enhanced by large factors (in some cases by $>10^6$) towards molecular outflows (Martín-Pintado, Bachiller & Fuente 1992). This is due to the injection of molecular material into the gas phase by the processing of dust grains (e.g. Caselli, Hartquist & Havnes 1997; Schilke et al. 1997; Guillet, Pineau des Forêts &

★E-mail: ijimenez-serra@cfa.harvard.edu
†Present address: Department of Astronomy, University of Florida, Gainsville, FL 32611, USA.

Jones 2007; Jiménez-Serra et al. 2008; Guillet, Jones & Pineau des Forêts 2009).

The typical SiO emission measured in molecular outflows shows broad line profiles with linewidths of some tens of km s^{-1} (Martín-Pintado et al. 1992). Narrower SiO lines have also been detected towards low-mass star-forming regions such as NGC1333 and L1448-mm (Lefloch et al. 1998; Jiménez-Serra et al. 2004). Although the nature of this emission is not clear yet, Lefloch et al. (1998) have proposed that these lines could trace shocked material deflected and decelerated by the interaction with pre-existing clumps. Alternatively, narrow SiO could arise from gas recently processed by the magnetic precursor of young magnetohydrodynamic (MHD) shocks (Jiménez-Serra et al. 2004).

In the case of IRDCs, Motte et al. (2007) and Beuther & Sridharan (2007) have recently carried out two large surveys of SiO emission towards the Cygnus X molecular cloud complex and towards a sample of IRDCs, respectively. Their single-pointing observations show that the detection rate of SiO towards IR-quiet massive cores close to sites of ongoing star formation is relatively high. This is expected since SiO is tightly associated and restricted to shocked gas in outflows. However, no widespread narrow SiO emission, as seen towards NGC1333, has been reported in IRDCs so far.

We present the detection of widespread SiO $J = 2\rightarrow1$ emission (size of $\geq$2 pc) towards the IRDC G035.39−00.33 (Cloud H in Butler & Tan 2009). From its filamentary morphology, this IRDC is believed to be at the early stages of its evolution as predicted by dynamical models of giant molecular cloud formation (van Loo et al. 2007; Hennebelle et al. 2008; Heitsch, Stone & Hartmann 2009). The observed large-scale SiO feature is probably a composition of broad and compact emission, linked to outflows associated with high-mass star formation, and extended narrow SiO emission. The observed narrow SiO lines could be explained (i) by a large-scale shock, remnant of the IRDC formation process, (ii) by decelerated or recently processed gas in the precursor of MHD shocks in large-scale outflows, probably driven by the 8 μm and 24 μm sources observed in the IRDC or (iii) by an undetected and widespread population of lower-mass protostars.

2 OBSERVATIONS AND RESULTS

The $J = 2\rightarrow1$ lines of SiO, CO, ^{13}CO and C^{18}O were mapped with the Instituto de Radioastronomía Milimétrica (IRAM) 30-m telescope at Pico Veleta (Spain) over an area of 2×4 arcmin^2 towards G035.39−00.33. These observations were carried out in 2008 August and in 2009 January and February. The large-scale molecular images were obtained in the on-the-fly (OTF) mode using the offsets (1830, 658), in arc seconds, for SiO, ^{13}CO and C^{18}O and (4995, 2828) for CO, as off-positions. The central coordinates of the map were α(J2000) = 18$^{\rm h}$57$^{\rm m}$08$^{\rm s}$, δ(J2000) = 02° 10′ 30″ ($l = 35\overset{\circ}{.}517$, $b = -0\overset{\circ}{.}274$). The SiO $J = 2\rightarrow1$ emission was mapped with the old Superconductor-Insulator-Superconductor (SIS) receivers, while the Heterodyne Receiver Array (HERA) multibeam receivers simultaneously observed the $J = 2\rightarrow1$ transitions of ^{13}CO and C^{18}O. The CO $J = 2\rightarrow1$ emission was mapped with the new generation Eight Mixer Receivers (EMIR). In addition, we carried out single-pointing observations of the SiO $J = 2\rightarrow1$ and $J = 3\rightarrow2$ emission with EMIR towards the offsets (0,20), (30,−30), (0,−80), (−10,70) and (−37,37). The former three positions correspond to the brightest SiO emission peaks observed towards the IRDC (Section 2.1). The latter two offsets show the regions where we have detected narrow SiO lines (Section 2.2). All receivers were tuned to single sideband with rejections of $\geq$10 dB. The beam sizes were 28 arcsec at 90 GHz for the SiO $J = 2\rightarrow1$ line, 19 arcsec at 130 GHz for the SiO $J = 3\rightarrow2$ emission and 11 arcsec at 230 GHz for the CO, ^{13}CO and C^{18}O $J = 2\rightarrow1$ lines. The VErsatile SPectrometer Assembly (VESPA) spectrometer provided spectral resolutions of 40 and 80 kHz, which correspond to velocity resolutions of ∼0.14 and 0.1 km s^{-1} at 90 and 230 GHz, respectively. Saturn was used to calculate the focus, and pointing was checked every 2 h on G34.3+0.2. Typical system temperatures ranged from 100 to 300 K. All intensities were calibrated in units of antenna temperature, $T_{\rm A}^{*}$. To convert these intensities into units of main-beam temperature, $T_{\rm mb}$, we have used efficiencies of 0.81, 0.74 and 0.63 for the EMIR data at ∼90, 130 and 230 GHz and of 0.52 for the HERA data at ∼230 GHz. All this information is summarized in Table 1.

Table 1. Observed molecular transitions and line frequencies, telescope beam sizes and beam efficiencies for the EMIR and HERA receivers at the IRAM 30-m telescope.

Transition	Frequency (MHz)	Beam size (arcsec)	Beam eff.
SiO $J = 2\rightarrow1$	86846.96	28	0.81
SiO $J = 3\rightarrow2$	130268.61	19	0.74
CO $J = 2\rightarrow1$	230538.00	11	0.63
^{13}CO $J = 2\rightarrow1$	220398.68	11	0.52
C^{18}O $J = 2\rightarrow1$	219560.36	11	0.52

Fig. 1 (central panel) presents the high-sensitivity map of the SiO $J = 2\rightarrow1$ emission integrated from 36 to 51.5 km s^{-1} (blue contours), and superimposed on the mass surface density map, with an angular resolution of 2 arcsec, reported by Butler & Tan (2009). The SiO $J = 2\rightarrow1$ map has been obtained by averaging the OTF dumps in the SiO beam of 28 arcsec and by using a Nyquist-sampled grid with a pixel size of 14 arcsec. The 2σ intensity level of SiO is shown in dashed contours. The location of the massive cores (crosses; Rathborne et al. 2006; Butler & Tan 2009), 24-μm sources (red open triangles; extracted from MIPSGAL images; Carey et al. 2009), 8-μm sources (red open circles), and 4.5-μm extended emission (green squares; called *green fuzzies* in Chambers et al. 2009) in this IRDC, is also shown. The flux lower limits of the 8- and 24-μm sources reported in Fig. 1 are $\geq$3.5 and $\geq$2 mJy, respectively. We note that the cavity-like structures seen around the 8-μm sources are produced by the fact that the extinction mapping technique of Butler & Tan (2009) cannot be applied in the vicinity of IR-bright sources.

From Fig. 1, we find that the SiO $J = 2\rightarrow1$ emission is widespread across the filament with a spatial extent of $\geq 150 \times 50$ arcsec^2. This corresponds to $\geq 2.1 \times 0.7$ pc^2 at a distance of ∼2.9 kpc (Rathborne et al. 2006). This size should be considered as a lower limit since SiO is also detected towards the north and northwest of Core MM7/H6 (see Section 2.2), and extends off to the south of the imaged area. The SiO map shows three bright condensations (marked N, E, S) surrounded by weaker, more extended emission that covers much of the IRDC filament.

In Fig. 1, we also report a sample of spectra of SiO $J = 2\rightarrow1$ and $J = 3\rightarrow2$, and of the CO, ^{13}CO and C^{18}O $J = 2\rightarrow1$ lines, measured towards several positions in the IRDC. Since single-pointing observations of SiO $J = 2\rightarrow1$ and $J = 3\rightarrow2$ were not carried out towards (10,10), the SiO $J = 2\rightarrow1$ spectrum reported in Fig. 1 was obtained by averaging the OTF data within the 28-arcsec beam of the IRAM 30-m telescope at ∼90 GHz. The spectra of CO and of its isotopologues shown in Fig. 1 have also been obtained following

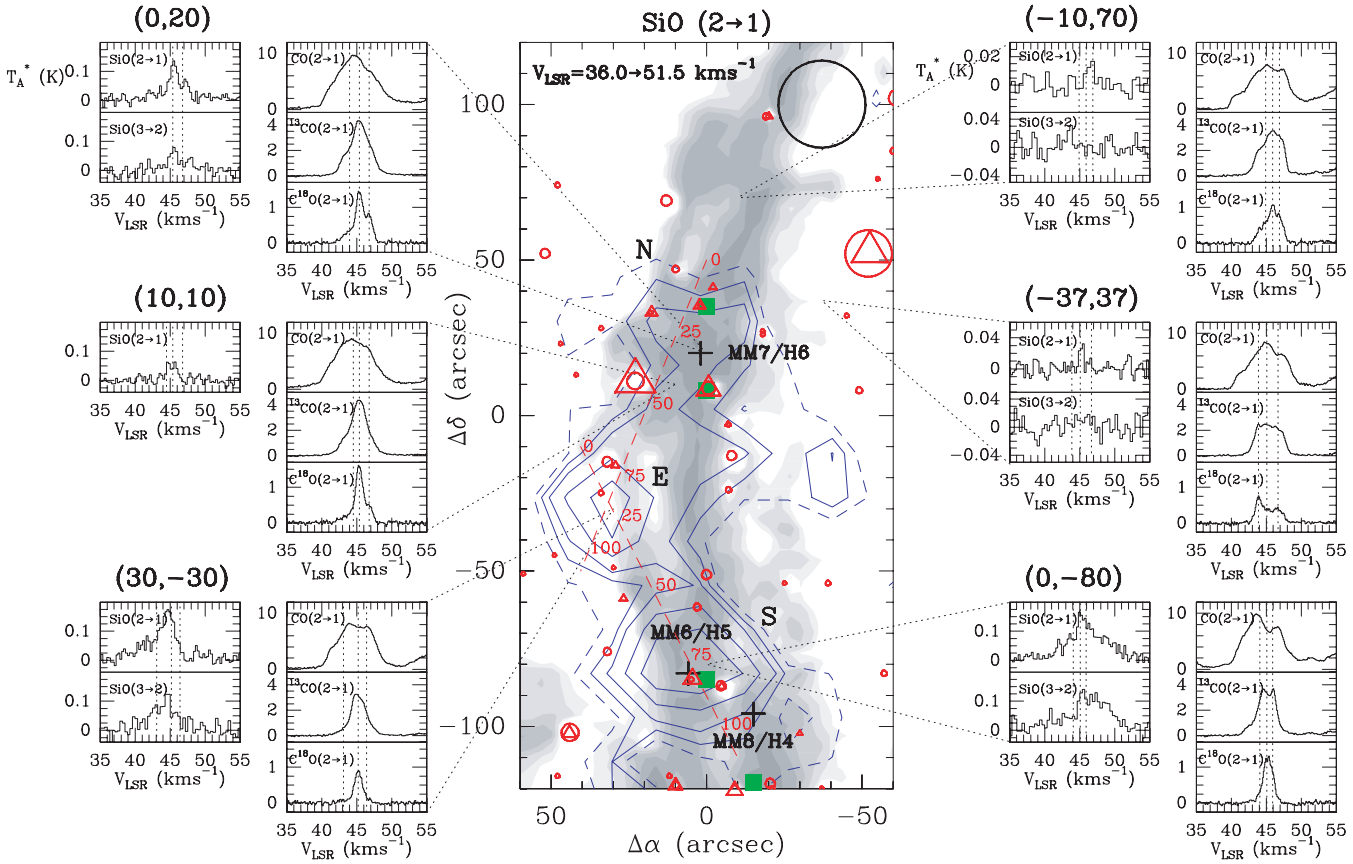

Figure 1. Central panel: integrated intensity map of the SiO $J = 2\rightarrow1$ line towards G035.39−00.33 for the velocity range from 36 to 51.5 km s^{-1} (blue contours), overlapped on the mass surface density map of Butler & Tan (2009, grey scale). The contour levels of the SiO emission are 10 (2σ; dashed contour), 15, 20, 30 and 40 mK km s^{-1}. For the mass surface density map, contours are 0.014 (2σ), 0.021, 0.035, 0.049, 0.07, 0.105 and 0.14 g cm^{-2},respectively. Crosses indicate the cores reported in the cloud by Rathborne et al. (2006) and Butler & Tan (2009). Red open circles, red open triangles and green squares show the location of the 8- and 24-μm sources (Carey et al. 2009) and 4.5-μm extended emission (Chambers et al. 2009) detected in G035.39−00.33, respectively. The marker sizes used for the 8- and 24-μm sources have been scaled by the source flux. Red dashed lines show the directions of the $P-V$ diagrams of Fig. 2. Red numbers indicate the distance (in arcseconds) along the cuts made for these diagrams. The SiO $J = 2\rightarrow1$ beam size is plotted at the upper-right corner. Left- and right-hand panels: sample of spectra of SiO $J = 2\rightarrow1$ and $J = 3\rightarrow2$, and of CO, ^{13}CO and C^{18}O $J = 2\rightarrow1$, measured towards several positions across the IRDC. The CO, ^{13}CO and C^{18}O spectra were obtained by averaging the OTF data within the 28-arcsec beam of the SiO $J = 2\rightarrow1$ observations. The vertical dotted lines show the velocities of the CO filaments, as calculated from the C^{18}O $J = 2\rightarrow1$ emission (Table 2 and Section 2.3).

this procedure. From the SiO spectra, we find that SiO shows a wide variety of line profiles, from broad emission with redshifted and/or blueshifted line wings [see offsets (0,20), (30,−30) and (0,−80)] to narrow lines peaking at the ambient cloud velocity $v_{\rm LSR} \sim 45$ km s^{-1} [offsets (10,10), (−10,70) and (−37,37)]. The CO, ^{13}CO and C^{18}O lines show three different velocity components centred at $v_{\rm LSR}$ ∼44, 45 and 47 km s^{-1} (see Section 2.3).

In Table 2, we report the observed parameters (central radial velocity, $v_{\rm LSR}$, linewidth, Δv, and peak intensity, $T_{\rm A}^*$) of the different velocity components measured in SiO $J = 2\rightarrow1$, SiO $J = 3\rightarrow2$ and C^{18}O $J = 2\rightarrow1$ (representative of the low-density CO gas) towards (0,20), (10,10), (30,−30), (−10,70), (−37,37) and (0,−80). These parameters were obtained by fitting the molecular line emission with three Gaussian line profiles simultaneously. Although this method works better for the C^{18}O $J = 2\rightarrow1$ emission, the Gaussian linewidths derived from the SiO $J = 2\rightarrow1$ line profiles provide a rough estimate of the velocity range extent and terminal velocities of the shocked SiO emission. In Table 2, the errors in $v_{\rm LSR}$ and Δv correspond to those obtained from the multicomponent Gaussian fit. For the errors in the peak intensities, $T_{\rm A}^*$, we consider the noise rms ($1\sigma_{\rm rms}$) of the spectra in Fig. 1 and for the upper limits the $3\sigma_{\rm rms}$ noise level of this emission.

2.1 The broad SiO line emission towards condensations N, E and S

Fig. 1 shows that the brightest SiO $J = 2\rightarrow1$ and $J = 3\rightarrow2$ emission in the IRDC arises from three major condensations towards (0,20) [N], (30,−30) [E] and (0,−80) [S]. The N and S condensations peak at the densest cores reported in the filament (MM7/H6 and MM6/H5; Rathborne et al. 2006; Butler & Tan 2009), and harbour not only several 8- and 24-μm sources but also 4.5-μm extended emission (likely related to H_2 shocked gas; Noriega-Crespo et al. 2004). This suggests that these condensations are active sites of star formation.

Condensation E, however, is located east of the IRDC and slightly off the high-extinction region (see Fig. 1). Although small amounts of gas are present, no local maxima is seen towards E in either extinction (Butler & Tan 2009) or other high-density molecular tracers such as N_2H^+ or $H^{13}CO^+$ (Caselli et al., in preparation).

Table 2. Observed parameters of the SiO $J = 2 \rightarrow 1$ and $J = 3 \rightarrow 2$ lines, and of the $J = 2 \rightarrow 1$ emission of $C^{18}O$, towards several offsets in IRDC G039.35−00.33.

Molecule	Offsets (0,20)			(10,10)			(30,−30)		
	v_{LSR} (km s^{-1})	Δv (km s^{-1})	T_A^* (K)	v_{LSR} (km s^{-1})	Δv (km s^{-1})	T_A^* (K)	v_{LSR} (km s^{-1})	Δv (km s^{-1})	T_A^* (K)
SiO(2→1)	∼44.0	–	≤0.03	44.73(8)	0.7(2)	0.07(1)	42.9(4)	7.0(8)	0.06(1)
	45.56(6)	1.3(2)	0.13(1)	45.7(1)	0.8(3)	0.06(1)	44.73(7)	1.9(2)	0.12(1)
	47.30(8)	1.0(2)	0.07(1)	∼46.8(2)	–	≤0.04	∼46.4	–	≤0.04
SiO(3→2)	∼43	–	≤0.04	–	–	–	42.9(3)	3(1)	0.06(2)
	45.5(1)	1.7(4)	0.07(1)	–	–	–	44.9(2)	2.3(6)	0.08(2)
	47.8(2)	0.8(3)	0.05(1)	–	–	–	∼46.4	–	≤0.05
$C^{18}O$(2→1)	44.0(2)	2.3(3)	0.34(3)	44.500(1)	3.0(4)	0.25(4)	43.1(2)	1.7(4)	0.08(3)
	45.41(1)	1.08(4)	1.30(3)	45.38(1)	1.07(3)	1.36(4)	45.21(2)	1.30(3)	0.87(3)
	46.77(2)	1.26(5)	0.78(3)	46.78(8)	1.4(1)	0.36(4)	46.4(1)	1.4(3)	0.09(3)
		(−10,70)			(−37,37)			(0,−80)	
SiO(2→1)	∼44.9	–	≤0.018	∼43.9	–	≤0.03	43.2(3)	6.2(3)	0.04(1)
	∼45.9	–	≤0.018	45.3(1)	0.8(3)	0.04(1)	45.6(3)	2.9(3)	0.11(1)
	46.5(2)	1.5(4)	0.021(6)	∼46.7	–	≤0.03	49.1(3)	3.5(3)	0.06(1)
SiO(3→2)	∼44.9	–	≤0.04	∼43.9	–	≤0.05	∼43.2	–	≤0.07
	∼45.9	–	≤0.04	∼45.1	–	≤0.05	45.3(1)	0.9(3)	0.07(2)
	∼46.9	–	≤0.04	∼46.7	–	≤0.05	47.5(5)	4.8(9)	0.11(2)
$C^{18}O$(2→1)	44.9(1)	2.2(2)	0.57(3)	43.9(1)	1.1(1)	0.69(3)	44.097(8)	2.4(4)	0.13(3)
	45.89(3)	0.8(1)	0.60(3)	45.1(1)	1.2(1)	0.33(3)	45.07(2)	1.22(3)	1.07(3)
	46.92(5)	1.34(9)	0.68(3)	46.7(1)	1.7(1)	0.40(3)	45.92 (3)	1.04(6)	0.56(3)

Like N and S, several 8-μm sources are detected towards this condensation, but only one is seen at 24 μm and this is about 15 arcsec north of the peak SiO position (see Fig. 1). The *Spitzer* IRAC (Infrared Array Camera; 3–8 μm) and MIPS (Multiband Imaging Photometer for Spitzer; 24 μm) fluxes of this source are consistent with a protostellar model with a luminosity of $\sim 2 \times 10^4\,L_\odot$, negligible circumstellar material and a foreground extinction of $A_V = 15$ mag. This corresponds to a 15-$M_\odot$ star on the zero-age main sequence (ZAMS). This is the best-fitting model returned from the spectral energy distribution (SED) fitting program of Robitaille et al. (2007). However, this result is not unique and the determination of protostellar properties from a relatively poorly constrained SED is quite uncertain. For example, the observed luminosity across the IRAC bands is only $\sim 20\,L_\odot$, and the above estimate of a much higher luminosity relies on the reality of the large foreground extinction. The source in condensation E could be responsible for the SiO broad feature observed towards this condensation. However, one would not expect strong outflow activity from such an evolved star. Alternatively, this source could be of much lower luminosity and mass and has more active accretion and outflow activity. There may also be other low-luminosity protostars in the vicinity, although the lack of high enough angular resolution in our SiO images prevents to establish if this is the origin of the broad SiO emission in this condensation (see below).

In Fig. 2, we show the $P-V$ diagrams of the SiO $J = 2 \rightarrow 1$ emission observed between the N and E and the E and S condensations, for the velocity range from 40 to 50 km s^{-1}. Outside this velocity range, the emission of SiO $J = 2 \rightarrow 1$ is below the 2σ rms level in the spectra. From Fig. 2, we find that the typical SiO line profiles towards condensations N, E and S have a central component peaking at $v_{LSR} \sim 45$ km s^{-1}, with broader line wing emission. The linewidths of the central component are ∼1–3 km s^{-1}, and those of the broad SiO emission are ∼4–7 km s^{-1} (Table 2). The blueshifted and redshifted terminal velocities are ∼40 and 50 km s^{-1}, respectively (i.e. ±5 km s^{-1} with respect to the central velocity $v_{LSR} \sim 45$ km s^{-1}; Fig. 1). While the broad SiO emission

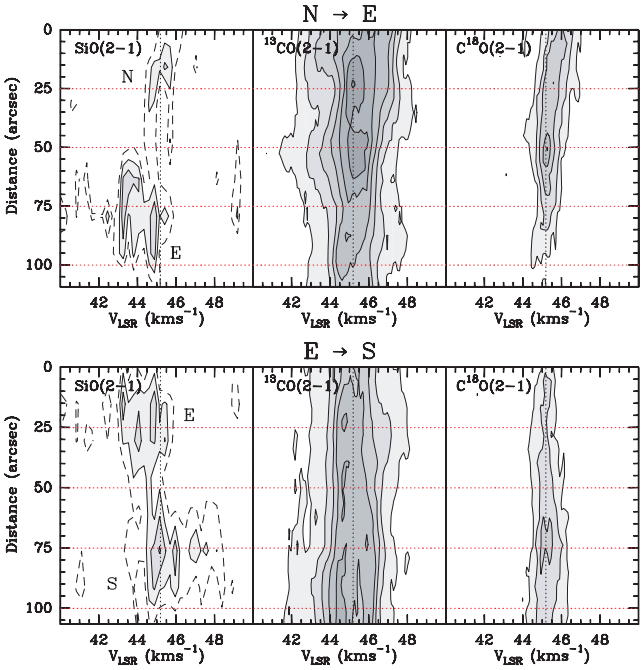

Figure 2. $P-V$ diagrams of the SiO, ^{13}CO and $C^{18}O$ $J = 2 \rightarrow 1$ emission (in units of T_A^*), obtained along the lines linking condensations N, E and S (see red dashed lines and red numbers in Fig. 1). The distance (in arcseconds) shown in the *y*-axis corresponds to that measured along these lines from north to south (see also horizontal red dotted lines in this figure). The contour levels for SiO $J = 2 \rightarrow 1$ are 60 (2σ; dashed contours), 90, 120 and 150 mK. For ^{13}CO and $C^{18}O$, the first contour and level step are 0.48 (3σ) and 0.8 K for ^{13}CO $J = 2 \rightarrow 1$ and 0.48 (3σ) and 0.48 K for $C^{18}O$ $J = 2 \rightarrow 1$. While the beam size of the SiO $J = 2 \rightarrow 1$ data is 28 arcsec, the angular resolution used in the $P-V$ diagrams of the ^{13}CO and $C^{18}O$ $J = 2 \rightarrow 1$ lines is 11 arcsec.

towards condensation E is blueshifted, the SiO line wings towards N and S mainly appear at redshifted velocities. Broad line profiles have previously been reported in SiO and other molecular species such as H_2CO and CH_3OH towards several samples of IRDCs (see Carey et al. 1998; Beuther & Sridharan 2007; Leurini et al. 2007; Sakai et al. 2008), and are believed to trace material associated with molecular outflows.

The SiO $P-V$ diagram of Fig. 2 also shows that condensations N, E and S have several local maxima centered at different radial velocities. Due to the low angular resolution of our SiO observations, it is currently impossible to determine whether these maxima are produced by error fluctuations in the SiO line temperature or whether they are associated with shocked gas high-velocity *bullets* or with different low-mass protostars (see Section 4).

The $P-V$ diagrams of ^{13}CO $J = 2\rightarrow1$ (Fig. 2) show that the terminal velocities of the ^{13}CO lines are, in general, similar to those measured for SiO towards the condensations N, E and S. The C^{18}O $J = 2\rightarrow1$ emission does not reveal any significant broad line wing emission since it is mainly associated with the high-density gas seen in extinction towards G035.39−00.33 (see Section 2.3). The correlation between the CO molecular gas and the mass surface density map of Butler & Tan (2009) will be analysed in detail in the near future (Hernandez et al., in preparation).

2.2 The extended and narrow SiO components

In addition to the broad SiO condensation N, E and S, the $P-V$ diagrams of Fig. 2 show that very narrow SiO emission [with linewidths of $\leq$1 km s^{-1}; offset (10,10) in Fig. 1] arises from regions linking these condensations. This is more clearly seen in Fig. 3 (central panel), where the narrow SiO lines arising from ambient gas (at $v_{\rm LSR} \sim 45$ km s^{-1}) form a large-scale and extended *ridge* that follows the filament. We note that the SiO emission associated with the ridge shows narrower line profiles than C^{18}O $J = 2\rightarrow1$ [0.8 km s^{-1} versus ∼1–3 km s^{-1}; offset (10,10) in Table 2]. The peak intensity of narrow SiO towards this position is relatively weak (0.06 K; Table 2) and is at the ∼5σ level (the $\sigma_{\rm rms}$ of the SiO $J = 2\rightarrow1$ spectrum is 0.012 K; Fig. 1).

The high-sensitivity single-pointing SiO spectra obtained with EMIR towards (−10,70) and (−37,37) also reveal that the

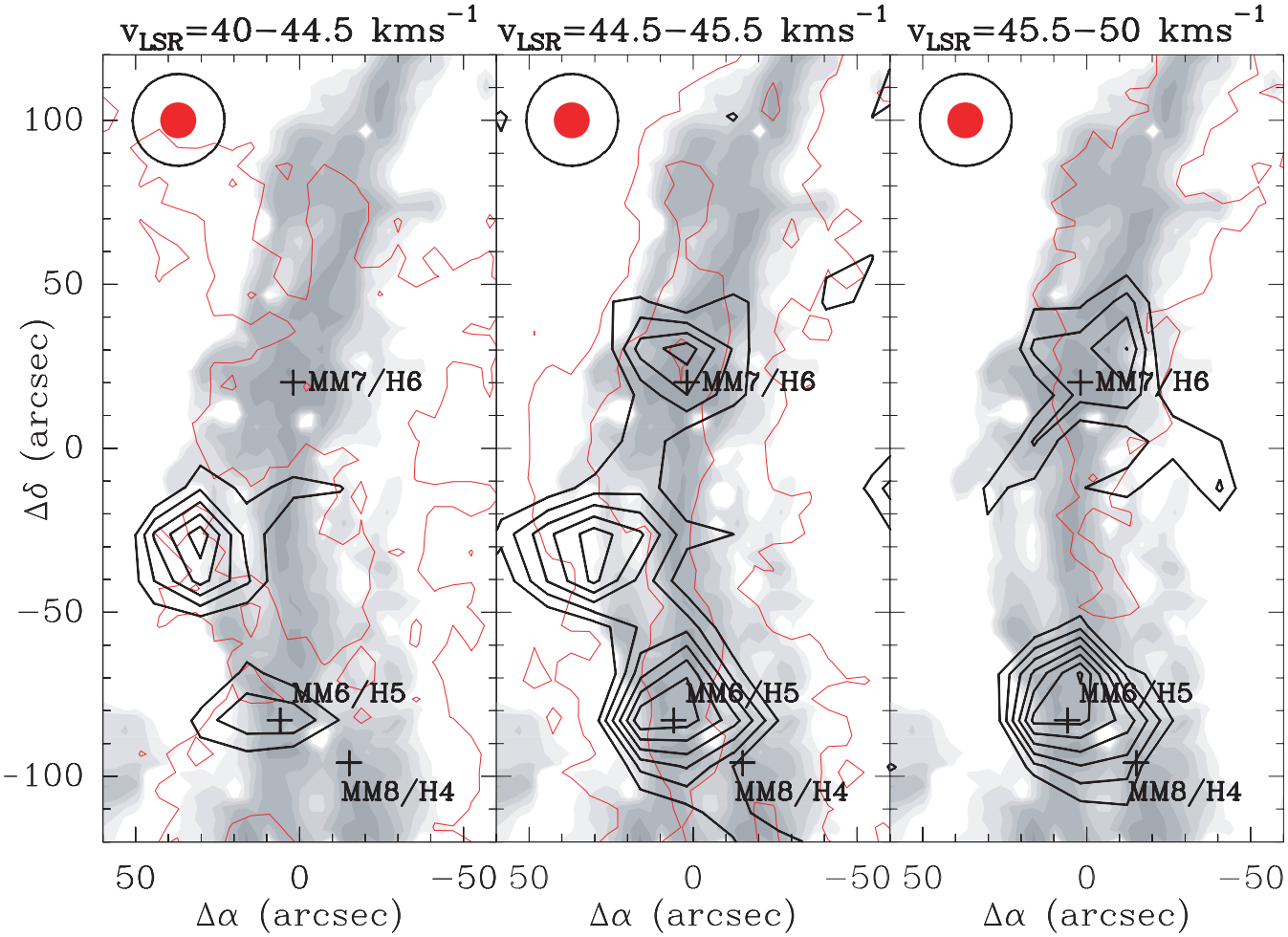

Figure 3. Integrated intensity maps (in units of $T_{\rm A}^{*}$ km s^{-1}) of the SiO $J = 2\rightarrow1$ (black contours) and C^{18}O $J = 2\rightarrow1$ lines (red contours) measured towards G035.39−00.33 from 40 to 44.5 km s^{-1} (blueshifted gas; left-hand panel), 44.5 to 45.5 km s^{-1} (ambient gas; central panel) and 45.5 to 50 km s^{-1} (redshifted gas; right-hand panel). The mass surface density map (Butler & Tan 2009) is shown in grey-scale (contour levels as in Fig. 1). The contour levels of the SiO $J = 2\rightarrow1$ maps are 24 (3σ), 32, 40, 48 and 56 mK km s^{-1} for the blueshifted emission, 51 (3σ), 68, 85, 102, 119 and 136 mK km s^{-1} for the ambient velocity range and 27 (3σ), 36, 45, 54, 63, 72 and 81 mK km s^{-1} for the redshifted gas. For clarity, we only plot the contours at the 5σ, 15σ and 25σ levels in the C^{18}O maps, with first contours at 150, 350 and 200 mK km s^{-1} for the blueshifted (left-hand panel), ambient (centre panel) and redshifted (right-hand panel) velocity ranges, respectively. Beam sizes of the SiO $J = 2\rightarrow1$ (black circle) and C^{18}O $J = 2\rightarrow1$ observations (filled red circle) are indicated in the upper-left corner.

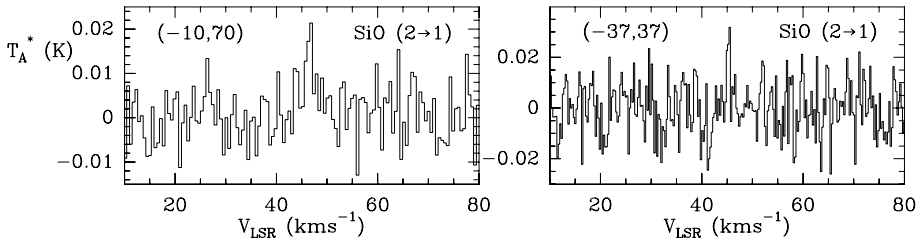

Figure 4. High-sensitivity SiO $J = 2\rightarrow1$ spectra measured with EMIR towards (−10,70) and (−37,37). The rms is 6 mK for the (−10,70) spectrum and 10 mK for the (−37,37) observation.

narrow SiO component spreads north and northwest of Core MM7/H6 (Fig. 4). The SiO data towards (−10,70) have been smoothed to a velocity resolution of 0.53 km s^{-1} to improve the signal-to-noise ratio of the spectrum. For the (−37,37) offset, however, we keep a velocity resolution of 0.26 km s^{-1}, because the SiO line emission towards this position is a factor of 2 narrower than that reported towards (−10,70) (i.e. 0.8 versus 1.5 km s^{-1}; see Table 2). The narrow SiO lines are very faint and have integrated line intensities of 0.038 ± 0.005 and 0.030 ± 0.005 K km s^{-1} towards (−10,70) and (−37,37), respectively. Since the SiO lines reported by Beuther & Sridharan (2007) in a sample of IRDCs have significantly larger linewidths (≥2.5 km s^{-1}) than those observed towards the ridge, towards (−10,70) or towards (−37,37), these lines are the narrowest features detected so far in a high-mass star-forming region. The SiO $J = 3\rightarrow2$ lines are not detected towards positions (−10,70) and (−37,37).

From the weak intensity and spatial distribution of narrow SiO, one could think that this emission could be due to some line emission contribution, within the large 30-m beam of our observations (∼28 arcsec), arising from condensations N, E and S. However, the narrow SiO lines measured towards (10,10), (−10,70) and (−37,37) have line profiles different from those observed towards N, E and S (see Fig. 1), and their central radial velocities differ from those found towards these condensations. This is particularly clear towards (−10,70), where the line peak velocity of narrow SiO is redshifted by ∼1 km s^{-1} with respect to that derived towards N. Therefore, the narrow SiO lines detected in G035.39−00.33 trace different molecular material from that seen in the SiO condensations N, E and S.

Finally, in Fig. 1, we note that the narrow SiO emission towards (−10,70) and (−37,37) lies below the 2σ contour level of the integrated intensity SiO map. This is due to the fact that narrow SiO lines are diluted in the broad velocity range considered to create the map. In Fig. 3 (central panel), the narrow SiO emission detected towards (−10,70) with the high-sensitivity EMIR receivers (Fig. 4) also lies below the 3σ noise level of the SiO map at ambient velocities, because the observations with the old SIS receivers were not sensitive enough to detect such faint emission (see above). The narrow SiO lines towards (−10,70) are of particular interest because they do not show any clear association with a 8- or 24-μm source. The narrow SiO emission detected towards (−37,37) is likely associated with the faint SiO condensation (intensity level of ∼3σ) located at (−40,50) in the central panel of Fig. 3.

2.3 The CO filaments in G035.39−00.33

The general kinematics of the low-density CO gas towards G035.39−00.33, as traced by $C^{18}O$ $J = 2\rightarrow1$, are also shown in Fig. 3. The CO gas is distributed along three different filaments with radial velocities v_{LSR} = 44.1, 45.3 and 46.6 km s^{-1}. These values correspond to the averaged central radial velocities derived for every filament from the $C^{18}O$ $J = 2\rightarrow1$ Gaussian fit parameters shown in Table 2. While the central and brightest filament at $v_{LSR} \sim 45$ km s^{-1} bends east tightly following the densest material within the IRDC, the blueshifted filament with $v_{LSR} \sim 44$ km s^{-1} intersects the former one in an arc-like structure pointing west (i.e. with the centre of curvature lying to the east of the IRDC). The two intersecting regions are coincident with the highest density cores reported in the IRDC, MM7/H6, MM6/H5 and MM8/H4 (Rathborne et al. 2006; Butler & Tan 2009). Although not as clear as for the blueshifted CO component,the redshifted filament with $v_{LSR} \sim 47$ km s^{-1} seems to further bend east with respect to the central one, following the trend already shown by the latter filament. The morphology of these filaments resembles the molecular structures predicted by flow-driven, shock-induced and magnetically-regulated models of cloud formation (see e.g. Fiege & Pudritz 2000a,b; van Loo et al. 2007; Hennebelle et al. 2008; Heitsch et al. 2009). As discussed in Section 4, in these scenarios the high-density filament seen in extinction would have been formed in a cloud–cloud collision, with the low-density CO filaments still accreting material on to it. The kinematics and excitation of the low-density CO gas will be described in a forthcoming paper (Jiménez-Serra et al., in preparation).

3 EXCITATION AND FRACTIONAL ABUNDANCES OF SiO

Except for the (10,10) position, where SiO $J = 3\rightarrow2$ single-dish observations were not carried out (see Section 2), we can derive the H_2 densities of the gas, $n(H_2)$, and the excitation temperatures, T_{ex}, and column densities of SiO, N(SiO), from the SiO $J = 3\rightarrow2/J = 2\rightarrow1$ intensity ratio and by using the large velocity gradient (LVG) approximation. As shown in Section 3.3, the validity of this approximation is provided by the fact that the SiO line emission towards G035.39−00.33 is optically thin. We assume that the SiO $J = 2\rightarrow1$ and $J = 3\rightarrow2$ lines trace the same material.

3.1 LVG modelling and input parameters

In our LVG calculations, we have considered the first 15 rotational levels of SiO and used the collisional coefficients of SiO with H_2 derived by Turner et al. (1992) for temperatures up to $T = 300$ K. These collisional coefficients are well suited for our case of study, because the kinetic temperatures assumed for the SiO shocked gas in the IRDC are $T \ll 300$ K. As input parameters, we have considered the cosmic microwave background temperature (i.e. T_{bg} = 2.7 K), the linewidths of the SiO emission and the kinetic temperature of the gas, T_{kin}. The brightness temperature, T_B, excitation temperature, T_{ex}, and optical depth, τ(SiO), of every rotational line transition of SiO are then calculated for a grid of models with

different H_2 (volumetric) gas densities and column densities of SiO. We note that T_{ex} may significantly differ from T_{kin}, since the excitation conditions of the SiO shocked gas could be far away from the local thermodynamic equilibrium (LTE).

Three different velocity regimes have been considered for the SiO emission observed in G035.39−00.33: the ambient component, which ranges from 44.5 to 45.5 km s^{-1}; the moderate shocked gas, with 42.5 $\leq v_{LSR} <$ 44.5 km s^{-1} or 45.5 $< v_{LSR} \leq$ 47.5 km s^{-1}, and the high-velocity regime, with $v_{LSR} <$ 42.5 km s^{-1} or $v_{LSR} >$ 47.5 km s^{-1}. Within every velocity regime, we perform the LVG calculations for velocity bins of 1 km s^{-1}. We assume that T_{kin} = 15 K for the ambient component (similar to those derived in a sample of IRDCs; Pillai et al. 2007) and T_{kin} = 25 and 45 K for the moderate and high-velocity SiO gas, respectively. The latter two temperatures are consistent with those found in the shocked gas of the L1448-mm outflow (Jiménez-Serra et al. 2005).

We would like to stress that the selection of these temperatures is expected not to be crucial in our calculations of N(SiO), since the excitation of the SiO rotational lines with $J_{up} < 5$ does not strongly depend on T_{kin} but on the H_2 density of the gas (Nisini et al. 2007). Indeed, if we increase T_{kin} from 15 to 50 K for the narrow SiO component and from 25–45 to 300 K for the moderate- and high-velocity SiO shocked gas, the derived N(SiO) change by less than a factor of 2.

The brightness temperatures, T_B, derived with the LVG model for the SiO $J = 2\rightarrow1$ and $J = 3\rightarrow2$ lines are finally compared with those observed towards G035.39−00.33, in units of T_{mb}. We assume that the SiO emission is uniformly distributed and that the beam-filling factor of our SiO observations is ∼1 (only in this case $T_B \sim T_{mb}$). This is justified by the fact that the SiO emission is extended in the IRDC.

To derive the SiO fractional abundances, the H_2 column densities were estimated from C^{18}O for the ambient gas, from ^{13}CO for the moderate-velocity regime and from CO for the high-velocity gas. In contrast with the mass surface density map of Butler & Tan (2009), which gives an averaged value of the H_2 column density of the gas towards a certain position, CO and its isotopologues provide estimates of the H_2 column density as a function of velocity within the shock. We assume isotopic ratios ^{12}C/^{13}C = 53 and ^{16}O/^{18}O = 327 (Wilson & Rood 1994) and a CO fractional abundance of 2 × 10^{-4} across the IRDC. The uncertainty in the CO abundance is about a factor of 2, considering its variations in different molecular cloud complexes (e.g. Frerking, Langer & Wilson 1982) as well as within the same complex (Pineda, Caselli & Goodman 2008). The value adopted in this study is close to that directly measured towards another high-mass star-forming region (NGC2024; Lacy et al. 1994), which better represents the properties of IRDCs.

3.2 LVG results

The T_{ex} and SiO fractional abundances, χ(SiO), derived towards (−10,70), (−37,37), (0,20), (30,−30) and (0,−80) by means of the LVG approximation, are shown in Fig. 5. Towards (10,10), χ(SiO) was calculated assuming that T_{ex} = 9 K [i.e. similar to those derived towards (−10,70) and (−37,37); see below] and that the SiO emission is optically thin.

For the narrow SiO emission towards (−10,70) and (−37,37), we obtain $T_{ex} \sim$ 9 K, optical depths τ(SiO) ≤ 0.01 and SiO column densities ranging from 5 × 10^{10} to 10^{11} cm^{-2}. This implies SiO fractional abundances χ(SiO) ∼ 6–7 × 10^{-11} (Fig. 5). The derived H_2 gas densities are ≤6 × 10^5 cm^{-3}. Towards (10,10), the derived SiO fractional abundance is ∼5 × 10^{-11}. These abundances are

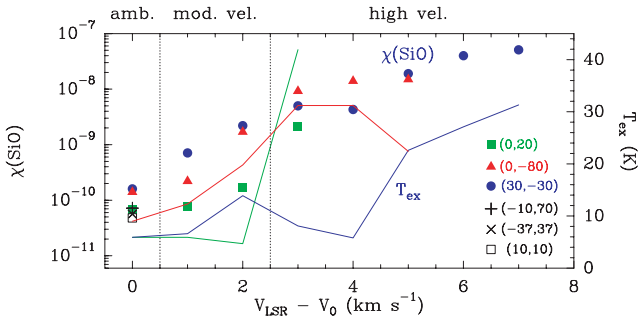

Figure 5. Excitation temperatures, T_{ex} (colour lines), and SiO fractional abundances, χ(SiO) (symbols), derived for the ambient, moderate and high-velocity regimes (vertical dotted lines) observed towards several offsets in G035.39−00.33. We consider v_0 = 45.0 km s^{-1}. The errors associated with T_{ex} are estimated to range from 15 to 35 per cent.

a factor of 10 larger than the upper limits found in dark clouds (≤10^{-12}; Ziurys et al. 1989; Requena-Torres et al. 2007) and are similar to those measured from narrow SiO towards the molecular outflows in the low-mass star-forming regions NGC1333 and L1448-mm (Lefloch et al. 1998; Jiménez-Serra et al. 2004).

Towards the N, E and S condensations, T_{ex} and χ(SiO) tend to increase from the ambient to the moderate- and the high-velocity regimes (Fig. 5). The typical optical depths derived for the SiO emission in these condensations are τ(SiO) ≤ 0.06. The derived H_2 gas densities and SiO column densities range from 10^5 to 10^6 cm^{-3} and from 5 × 10^{10} to 4 × 10^{11} cm^{-3}, respectively. For T_{ex}, a similar behaviour for the excitation of the SiO shocked gas has been reported towards the L1157-mm and L1448-mm outflows (Nisini et al. 2007), where the SiO $J = 8\rightarrow7/J = 5\rightarrow4$ ratio is known to increase as a function of velocity within the shock (Nisini et al. 2007). In the case of the SiO fractional abundances, χ(SiO) is progressively enhanced from ∼10^{-10} in the ambient gas to ∼10^{-9} in the moderate-velocity component and to ≥10^{-8} in the high-velocity shocked gas. This trend has also been observed towards the L1448-mm outflow (Jiménez-Serra et al. 2005).

Although the LVG model does not provide the errors associated with T_{ex}, we can roughly estimate them from the integrated intensity ratio between the SiO $J = 3\rightarrow2$ and the SiO $J = 2\rightarrow1$ transitions. The errors range from 15 to 35 per cent. This range corresponds to the change in signal-to-noise ratio going from the strong SiO lines at ambient velocities to the fainter SiO emission at the moderate- and high-velocity shock regimes.

3.3 Validity of the LVG approximation

As shown in Section 3.2, the typical optical depths derived for the SiO emission towards G035.39−00.33, are τ(SiO) ≪ 1. In molecular outflows, the SiO line emission is expected to be optically thin for ratios N(SiO)/$\Delta v < 5 \times 10^{13}$ cm^{-2} km^{-1} s, where N(SiO) is the derived SiO column density and Δv is the linewidth of the SiO line profiles (Nisini et al. 2007). The derived SiO column densities, N(SiO), towards the IRDC are relatively low and range from 5 × 10^{10} to 4 × 10^{11} cm^{-2} (Section 3.2). Considering that the velocity bins used in our calculations are 1 km s^{-1} wide, the ratio N(SiO)/Δv is 5 × 10^{10}–4 × 10^{11} cm^{-2} km^{-1} s, i.e. well below the upper limit established by Nisini et al. (2007). Therefore, the use of the LVG approximation in our case is fully justified.

3.4 Comparison of the SiO fractional abundances with shock modelling

By using the parametrized model of Jiménez-Serra et al. (2008) that mimics the steady-state physical structure of a perpendicular C-shock, we find that the low SiO fractional abundances of $\sim 10^{-11}$ associated with the narrow SiO emission in G035.39−00.33 could be generated by the sputtering of dust grains within C-shocks with $v_s \sim 12\,\mathrm{km\,s^{-1}}$. A minimum ion-neutral drift velocity of $v_d = |v_n - v_i| = 5\,\mathrm{km\,s^{-1}}$ is required to sputter SiO abundances of a few 10^{-11} from the icy mantles of dust grains, if a fractional abundance of 10^{-8} for SiO is present within the mantles (Jiménez-Serra et al. 2008). This SiO abundance is the same as that measured in the moderate-velocity SiO shocked gas in L1448-mm and believed to trace material recently released from the mantles of dust grains (Jiménez-Serra et al. 2005). If SiO were only present within the cores of dust grains, a shock velocity of $v_s \sim 30\,\mathrm{km\,s^{-1}}$, with an ion-neutral drift velocity of $v_d \sim 18\,\mathrm{km\,s^{-1}}$, would be required to reproduce the low SiO fractional abundances of few 10^{-11} for narrow SiO.

The progressive enhancement of the SiO fractional abundances from $\sim 10^{-10}$ to $\geq 10^{-8}$ towards the N, E and S condensations could be explained by the sputtering of the mantles of dust grains along the propagation of a C-shock with $v_s \sim 30\,\mathrm{km\,s^{-1}}$, as proposed for the L1448-mm outflow (Jiménez-Serra et al. 2008). However, we note that other mechanisms such as shattering or vaporization in non-dissociative J-shocks (Guillet et al. 2007, 2009) could additionally contribute to the processing of dust grains in these regions. The inclusion of those mechanisms in the currently available state-of-the-art shock descriptions might significantly change our understanding of the shocked SiO emission in molecular outflows.

The comparison of synthetic SiO line profiles (as derived from radiative transfer modelling) with the SiO line emission observed towards the IRDC lies outside the scope of this paper. The lack of high enough angular resolution in our SiO OTF maps indeed prevents to clearly establish the actual morphology and size of the SiO emitting regions, which are crucial parameters in the modelling of the SiO line profiles.

4 ON THE ORIGIN OF THE PARSEC-SCALE SIO EMISSION IN G035.39−00.33

Theoretical models of flow-driven (Hennebelle & Pérault 1999; Heitsch et al. 2006; Hennebelle et al. 2008; Heitsch et al. 2009), shock-induced (Koyama & Inutsuka 2000, 2002; van Loo et al. 2007) and magnetically-regulated formation of clouds (Fiege & Pudritz 2000a,b) predict that these regions have a very filamentary structure at their early stages of evolution. Consistent with this idea, the filamentary IRDC G035.39−00.33 shows a relatively high number of quiescent cores (without H_2 shocked gas or 24-μm sources), which are believed to be at a pre-stellar/cluster core phase (Chambers et al. 2009). As a consequence, one should not expect to find a significant impact of outflow interaction within the cores and on their surroundings (see e.g. Martín-Pintado et al. 1992; Beuther et al. 2002).

The high-sensitivity maps of the SiO emission towards G035.39−00.33, however, reveal for the first time that SiO is widespread along an IRDC. Large-scale SiO emission (with sizes ranging from 4 to 20 pc) has also been reported across the molecular clouds in the Galactic Centre (GC; Martín-Pintado et al. 1997; Amo-Baladrón et al. 2009). In this case, the origin of these lines is different from that in G035.39−00.33, because the SiO gas is highly turbulent (linewidths of ∼60–90 km s^{-1}). The large SiO fractional abundances ($\sim 10^{-9}$) derived towards these regions are likely generated in fast shocks of supernova explosions, H II regions and Wolf–Rayet stellar winds (Martín-Pintado et al. 1997), and/or associated with X-ray or cosmic ray induced chemistry (Amo-Baladrón et al. 2009). Besides the GC, the large-scale SiO emission observed towards this IRDC constitutes the largest SiO feature detected so far in a star-forming region.

In Section 2, we have shown that the SiO line profiles measured towards G035.39−00.33 have two different components with different spatial distributions, kinematics and excitation. The first one consists of bright and compact SiO condensations (N, E and S) with broad line profiles in both SiO $J = 2 \rightarrow 1$ and $J = 3 \rightarrow 2$ transitions. From our excitation and fractional abundance analysis of the SiO lines, T_{ex} and χ(SiO) tend to progressively increase for larger velocities within the shock (from 6 to 40 K and from $\sim 10^{-10}$ to $\geq 10^{-8}$, respectively), as expected for shocked gas in molecular outflows (Jiménez-Serra et al. 2005; Nisini et al. 2007). Towards N and S, this idea is supported by the detection of 8- and 24-μm sources (Carey et al. 2009) and extended H_2 shocked gas (Chambers et al. 2009) closely associated with these condensations. In addition, the observed spatial extent of the broad SiO emission is only ≤30 arcsec (i.e. ≤0.4 pc at 2.9 kpc), which is consistent with those measured in outflows associated with high-mass protostars towards other IRDCs (Fallscheer et al. 2009). We also note that this size is similar to the beam size of the SiO $J = 2 \rightarrow 1$ observations, for which the fractional abundances of SiO have been reproduced by our C-shock and sputtering models (Section 3.4).

For condensation E, we have seen that the broad SiO emission is not associated with any massive core in the region and is clearly off the high-extinction region (Rathborne et al. 2006; Butler & Tan 2009). In addition, no local maxima are seen in extinction or in other high-density molecular tracers in this region (Butler & Tan 2009, Caselli et al., in preparation). However, the IRAC 3–8 μm and the MIPS 24 μm fluxes of the source located 15 arcsec north of the SiO peak are consistent with a 15 $M_\odot$ star in the ZAMS. Although one would not expect strong outflow activity from such an evolved star, this source could be the origin of the broad SiO emission found in this condensation (Section 2.1). Indeed, the SiO fractional abundances derived towards E are the largest measured in G035.39−00.33 and are consistent with the idea that the SiO gas has been processed by a relatively strong shock (with $v_s \sim 30\,\mathrm{km\,s^{-1}}$; Section 3.4), similar to those found in outflows associated with high-mass star formation (see e.g. IRAS 20126+4104; Su et al. 2007). Therefore, although with the current data it is not possible to clearly establish the origin of broad SiO towards condensation E, it is likely that this emission is related to shocked outflowing gas.

The second SiO component detected towards G035.39−00.33 consists of extended and very narrow SiO emission that links condensations N, E and S and also spreads very faintly towards the north and northwest of Core MM7/H6. From the low SiO fractional abundances derived for this component ($\sim 10^{-11}$), the narrow SiO emission could be produced by the interaction of a large-scale low-velocity shock with $v_s \sim 12\,\mathrm{km\,s^{-1}}$ (Section 3.4) generated in the collision of two flows (Hennebelle & Pérault 1999; Heitsch et al. 2006; van Loo et al. 2007; Hennebelle et al. 2008; Heitsch et al. 2009). In G035.39−00.33, this collision could have been produced by the interaction between the main filament (as seen in the mass surface density map of Butler & Tan 2009) and the lower density filaments traced by $C^{18}O$ (see Fig. 3). Since the time-scales required for SiO to freeze out on to dust grains are relatively short (i.e. from 5×10^3 to 5×10^4 yr for volume densities from 10^5 to $10^4\,\mathrm{cm^{-3}}$;

see section 6.2 in Martín-Pintado et al. 1992), the dust grain processing event associated with this interaction would be relatively recent. The narrow feature would then constitute a signature of the filament–filament collision or of previous accretion events produced on to the main IRDC filament.

This scenario is supported not only by the extended morphology of narrow SiO but also by the fact that the coherent CO filaments observed towards G035.39−00.33 resemble the molecular structures predicted in these models (van Loo et al. 2007; Hennebelle et al. 2008; Heitsch et al. 2009). In addition, the narrow SiO lines, specially towards the north and northeast of Core MM7/H6, do not show any clear association with 8- or 24-μm sources (Section 2.2). However, we note that the relatively small (2–4 km s^{-1}) velocity difference between the CO filaments compared to the shock velocity of $\sim$12 km s^{-1} required to produce the low SiO fractional abundances of $\sim 10^{-11}$ does place constraints on this scenario. This would require that either much of the relative velocity between the colliding molecular gas is in the plane of the sky or much of the gas has already been decelerated in the interaction. Detailed comparison with the results of numerical simulations is required to assess the likelihood of these possibilities.

As proposed by Lefloch et al. (1998) for the NGC1333 low-mass star-forming region, the narrow SiO emission in G035.39−00.33 could arise from decelerated shocked gas associated with large-scale outflows driven by the 8- and 24-μm sources seen in the IRDC. This gas would have been decelerated by its interaction with a dense and clumpy surrounding medium (Lefloch et al. 1998). It is also possible that narrow SiO is produced by material recently processed in the magnetic precursor of MHD shocks, as proposed for the L1448-mm outflow (Jiménez-Serra et al. 2004). This idea is similar to that suggested by Beuther & Sridharan (2007), for which narrow SiO would be linked to the youngest jet/outflow objects present in their sample of IRDCs. As discussed by these authors, narrow SiO lines are unlikely to be produced by an effect of outflow inclination with respect to the line of sight, because this would lead to the detection of fewer outflows with broad line emission than outflows with narrow SiO (see section 3.2 in Beuther & Sridharan 2007). Although any of the previous mechanisms could explain the narrow SiO lines in the ridge between condensations N, E and S, it seems unlikely for offsets (−10,70) and (−37,37), where the narrow SiO lines do not show a clear association with 8- or 24-μm sources (Section 2.2).

Alternatively, the extended and narrow SiO emission towards G035.39−00.33 could be produced by a widespread and lower mass population of protostars, compared to those powering condensations N, E and S. Some of these distributed protostars may be visible as the 8-μm sources in Fig. 1, although we do see SiO emission from regions apparently devoid of such sources. In this scenario, beam dilution would then prevent us from detecting the broad SiO line wings expected to arise from these objects. Interferometric observations are thus needed to discriminate between (i) the large-scale shock scenario, remnant of the IRDC formation process, (ii) decelerated or recently processed gas in the precursor of MHD shocks in large-scale outflows driven by the 8- and 24-μm sources and (iii) an undetected and widespread lower mass protostar population, as an origin of the widespread SiO emission in G035.39−00.33.

Extended narrow SiO emission could also be produced by the UV photoevaporation of the mantles of dust grains in photon-dominated regions such as the Orion bar (Schilke et al. 2001). However, this mechanism seems unlikely in G035.39−00.33, because of the relatively low luminosity of the region (it is observed as an IR dark rather than bright cloud) and because the UV radiation field required to produce SiO fractional abundances similar to those observed in this cloud (of $\sim 10^{-11}$) should be at least few hundred times the Galactic UV field (Schilke et al. 2001). There is no evidence for sources capable of producing such an intense far-UV (FUV) field in this region, and even propagation of the much lower-intensity Galactic FUV radiation field into this cloud would be strongly impeded by its high extinction. Nor are cosmic ray induced UV photons (Gredel et al. 1989) expected to play a key role in the formation of narrow SiO since the same UV field is generated in nearby quiescent dark clouds, where no SiO is detected.

In summary, we report the detection of widespread (size of $\geq$2 pc) SiO emission towards a very filamentary IRDC. This emission presents two different components with different kinematics, excitation and spatial distributions. The compact morphology, large SiO fractional abundances and broad SiO line profiles observed towards N, E and S indicate that these condensations are shocked gas in outflows associated with high-mass star formation. The second SiO component is extended along the filament and shows very narrow line profiles, low SiO abundances and lower excitation than the gas detected towards N, E and S. Although interferometric images are needed to clearly establish the origin of this emission, the properties of narrow SiO are consistent with (i) a large-scale shock, remnant of the IRDC formation processes, (ii) decelerated or recently shocked material in the precursor of shocks in large-scale outflows powered by 8- and 24-μm sources or (iii) an undetected and widespread population of lower mass protostars.

ACKNOWLEDGMENTS

We acknowledge the IRAM staff, and in particular H. Wiesemeyer, for the help provided during the observations. We also thank Professor J. Martín-Pintado for helpful discussions on the different mechanisms that can produce widespread SiO in star-forming regions and an anonymous referee for his/her careful reading of the manuscript. JCT acknowledges support from NSF CAREER grant AST-0645412. FF acknowledges support by Swiss National Science Foundation grant (PP002 – 110504). This effort/activity is supported by the European Community Framework Programme 7, Advanced Radio Astronomy in Europe, grant agreement no.: 227290.

REFERENCES

Amo-Baladrón M. A., Martín-Pintado J., Morris M. R., Muno M. P., Rodríguez-Fernández N. J., 2009, ApJ, 694, 943
Beuther H., Sridharan T. K., 2007, ApJ, 668, 348
Beuther H., Schilke P., Sridharan T. K., Menten K. M., Walmsley C. M., Wyrowski F., 2002, A&A, 383, 892
Butler M. J., Tan J. C., 2009, ApJ, 696, 484
Carey S. J., Clark F. O., Egan M. P., Price S. D., Shipman R. F., Kuchar T. A., 1998, ApJ, 508, 721
Carey S. J. et al., 2009, PASP, 121, 76
Caselli P., Hartquist T. W., Havnes O., 1997, A&A, 322, 296
Chambers E. T., Jackson J. M., Rathborne J. M., Simon R., 2009, ApJS, 181, 360
Egan M. P., Shipman R. F., Price S. D., Carey S. J., Clark F. O., Cohen M., 1998, ApJ, 494, L199
Fallscheer C., Beuther H., Zhang Q., Keto E., Sridharan T. K., 2009, A&A, 504, 127
Fiege J. D., Pudritz R. E., 2000a, MNRAS, 311, 85
Fiege J. D., Pudritz R. E., 2000b, MNRAS, 311, 105
Frerking M. A., Langer W. D., Wilson R. W., 1982, ApJ, 262, 590
Gredel R., Lepp S., Dalgarno A., Herbst E., 1989, ApJ, 347, 289
Guillet V., Pineau des Forêts G., Jones A. P., 2007, A&A, 476, 263

Guillet V., Jones A. P., Pineau des Forêts G., 2009, A&A, 497, 145
Heitsch F., Slyz A. D., Devriendt J. E. G., Hartmann L. W., Burkert A., 2006, ApJ, 648, 1052
Heitsch F., Stone J. M., Hartmann L. W., 2009, ApJ, 695, 248
Hennebelle P., Pérault M., 1999, A&A, 351, 309
Hennebelle P., Banerjee R., Vázquez-Semadeni E., Klessen R. S., Audit E., 2008, A&A, 486, L43
Jiménez-Serra I., Martín-Pintado J., Rodríguez-Franco A., Marcelino N., 2004, ApJ, 603, L49
Jiménez-Serra I., Martín-Pintado J., Rodríguez-Franco A., Martín S., 2005, ApJ, 627, L121
Jiménez-Serra I., Caselli P., Martín-Pintado J., Hartquist T. W., 2008, A&A, 482, 549
Koyama H., Inutsuka S.-I., 2000, ApJ, 532, 980
Koyama H., Inutsuka S.-i., 2002, ApJ, 564, L97
Lacy J. H., Knacke R., Geballe T. R., Tokunaga A. T., 1994, ApJ, 428, L69
Lefloch B., Castets A., Cernicharo J., Loinard L., 1998, ApJ, 504, L109
Leurini S., Schilke P., Wyrowski F., Menten K. M., 2007, A&A, 466, 215
Martín-Pintado J., Bachiller R., Fuente A., 1992, A&A, 254, 315
Martín-Pintado J., de Vicente P., Fuente A., Planesas P., 1997, ApJ, 482, L45
Motte F., Bontemps S., Schilke P., Schneider N., Menten K. M., Broguiere D., 2007, A&A, 476, 1243
Nisini B., Codella C., Giannini T., Santiago García J., Richer J. S., Bachiller R., Tafalla M., 2007, A&A, 462, 163
Noriega-Crespo A., Moro-Martin A., Carey S., Morris P. W., Padgett D. L., Lalter W. B., Muzerolle J., 2004, ApJS, 154, 402
Pérault M. et al., 1996, A&A, 315, L165
Pillai T., Wyrowski F., Hatchell J., Gibb A. G., Thompson M. A., 2007, A&A, 467, 207
Pineda J. E., Caselli P., Goodman A. A., 2008, ApJ, 679, 481
Ragan S. E., Bergin E. A., Gutermuth R. A., 2009, ApJ, 698, 324
Rathborne J. M., Jackson J. M., Simon R., 2006, ApJ, 641, 389
Requena-Torres M. A., Marcelino N., Jiménez-Serra I., Martín-Pintado J., Martín S., Mauersberger R., 2007, ApJ, 655, L37
Robitaille T. P., Whitney B. A., Indebetouw R., Wood K., 2007, ApJS, 169, 328
Sakai T., Sakai N., Kamegai K., Hirota T., Yamaguchi N., Shiba S., Yamamoto S., 2008, ApJ, 678, 1049
Schilke P., Walmsley C. M., Pineau des Forêts G., Flower D. R., 1997, A&A, 321, 293
Schilke P., Pineau des Forêts G., Walmsley C. M., Martín-Pintado J., 2001, A&A, 372, 291
Su Y.-N., Liu S.-Y., Chen H.-R., Zhang Q., Cesaroni R., 2007, ApJ, 671, 571
Teyssier D., Hennebelle P., Pérault M., 2002, A&A, 382, 624
Turner B. E., Chan K.-W., Green S., Lubowich D. A., 1992, ApJ, 399, 114
van Loo S., Falle S. A. E. G., Hartquist T. W., Moore T. J. T., 2007, A&A, 471, 213
Wilson T. L., Rood R., 1994, ARA&A, 32, 191
Zhang Q., Wang Y., Pillai T., Rathborne J., 2009, ApJ, 696, 268
Ziurys L. M., Friberg P., Irvine W. M., 1989, ApJ, 343, 301

This paper has been typeset from a TEX/LATEX file prepared by the author.